ACS Catalysis

Research Article

Cite This: ACS Catal. 2020, 10, 66−72

pubs.acs.org/acscatalysis

Active Sulfur Sites in Semimetallic Titanium Disulfide Enable CO_2 Electroreduction

Abdalaziz Aljabour,[†] Halime Coskun,[†] Xueli Zheng,[‡,#] Md Golam Kibria,[‡,¶] Moritz Strobel,[§] Sabine Hild,[§] Matthias Kehrer,[∥] David Stifter,[∥] Edward H. Sargent,[‡] and Philipp Stadler*[,†,⊥,‡]

[†]Institute of Physical Chemistry, [§]Institute of Polymer Science, [∥]Center for Surface and Nanoanalytics, and [⊥]Linz Institute of Technology, Johannes Kepler University Linz, Altenbergerstrasse 69, 4040 Linz, Austria

[‡]Edward S. Rogers Sr. Department of Electrical and Computer Engineering, University of Toronto, 10 King's College Road, Toronto, Ontario M5S 3G4, Canada

Supporting Information

ABSTRACT: Electrocatalytic CO_2-to-CO conversion represents one pathway to upgrade CO_2 to a feedstock for both fuels and chemicals (CO, deployed in ensuing Fischer−Tropsch or bioupgrading). It necessitates selective and energy-efficient electrocatalysts—a requirement met today only using noble metals such as gold and silver. Here, we show that the two-dimensional sulfur planes in semimetallic titanium disulfide (TiS_2) provide an earth-abundant alternative. In situ Fourier transform infrared mechanistic studies reveal that CO_2 binds to conductive disulfide planes as intermediate monothiocarbonate. The sulfur−CO_2 intermediate state steers the reduction kinetics toward mainly CO. Using TiS_2 thin films, we reach cathodic energy efficiencies up to 64% at 5 mA cm^2. We conclude with directions for the further synthesis and study of semimetallic disulfides developing CO-selective electrocatalysts.

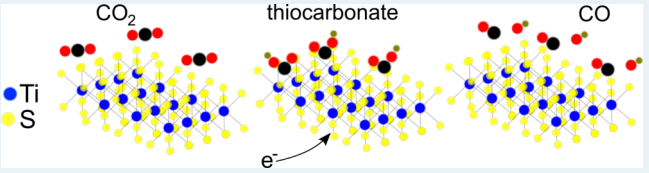

KEYWORDS: *CO_2 reduction reaction, titanium disulfide, electrocatalysis*

INTRODUCTION

Electrocatalysis is an attractive pathway to recycle CO_2, upgrading it using renewable energy.[1] Presently, the electrochemical CO_2-to-CO conversion process is the most efficient but requires catalyst materials with appreciable activity and selectivity to optimize energy efficiency.[2] Currently, these conditions are met by 4d and 5d transition metals such as Ag and Au.[3−7] Recent works have instead focused on the application of two-dimensional transition-metal dichalcogenides (2D-TMDCs) such as WSe_2 and MoS_2 with the goal of equaling the best CO_2-to-CO electrocatalyst performance,[8−17] but poor intrinsic conductivity and comparative complex synthesis are still subjects to be improved. Nonetheless, TMDCs are in general attractive electrocatalysts because more-earth-abundant metals with limited catalytic properties can be activated for electrochemical energy conversion.[14−16,18−24] We here follow particularly this hypothesis and replace the recently used Mo or W by the less electronegative 3d metal titanium. A similar concept has been recently demonstrated relying on nickel, iron, and tin oxides or sulfides where electronic properties were adapted for superior electrocatalytic performances.[25−28] Particularly, we found that titanium disulfide (TiS_2) is a promising candidate for CO_2-to-CO conversion because structurally it possesses cohesive van der Waals type of bonding similar to Mo- and W 2D-TMDCs but electronically has a narrow overlap of conduction and valence band (zero gap) and thus belongs to the class of semimetals with a conductivity similar to that of graphite.[29,30] We show here that TiS_2 can enhance CO_2 reduction because a major limitation in earlier used MoS_2 and related materials, the poor electrical conductivity, is resolved. We found that the increased conductivity activates a dangling site mechanism in the TiS_2 2D sulfur planes and as such exemplifies nonmetallic and CO-selective catalytic centers: here performed in situ Fourier transform infrared (FTIR) studies reveal that under cathodic bias, intermediates monothiocarbonates and thioles are formed. We show that in organic electrolytes, the intensity of the monothiocarbonate-based CO_2 reduction is favored over the competing hydrogen evolution, thus leading to a relative high selectivity for CO. Further, we found that the mechanism reported here is similar to earlier observations on conducting MoS_2 systems.[31] We demonstrate the selective electrosynthesis of CO at overpotentials less than 0.4 V at 5 mA cm^{-2} operation current density with a total Faradaic yield up to 83% using thin films of TiS_2 in the range of 200 nm. We tested the electrocatalyst in initial 16 h continuous operation electrolysis and found no significant degradation effects limiting the process. The electrocatalytic performance of TiS_2, that is, the selectivity for CO and the overpotential, can compete with other 3d-metal-based CO_2 catalysts.[25,28,32] We found that

Received: July 8, 2019
Revised: October 11, 2019
Published: October 24, 2019

DOI: 10.1021/acscatal.9b02872
ACS Catal. 2020, 10, 66−72

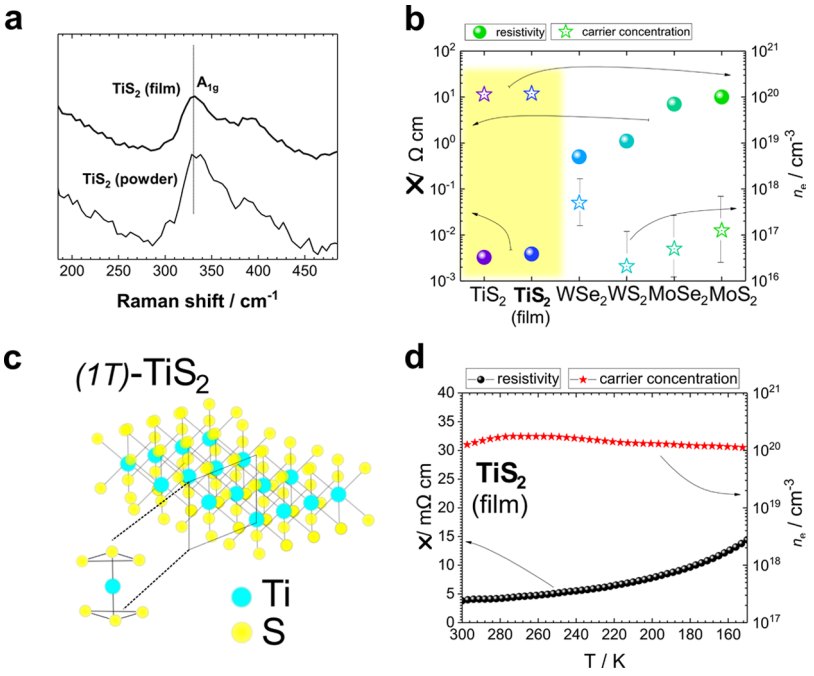

Figure 1. TiS_2 spectroscopic, structural, and electrical characterization. (a) Raman shift of (1T)-TiS_2 films show the characteristic band at 331 cm^{-1} (A_{1g} modes).[34] (b) Resistivities ρ (ascending order) and carrier concentrations of TiS_2 crystals and TiS_2 films compared to other TMDCs previously used as a CO_2 electrocatalyst.[4,35,36] (c) Schematic of TiS_2 structure (layered 1T-phase). (d) Temperature-dependent Hall effect and resistivity ρ of TiS_2 films show negative TCR and constant carrier concentration n_e.

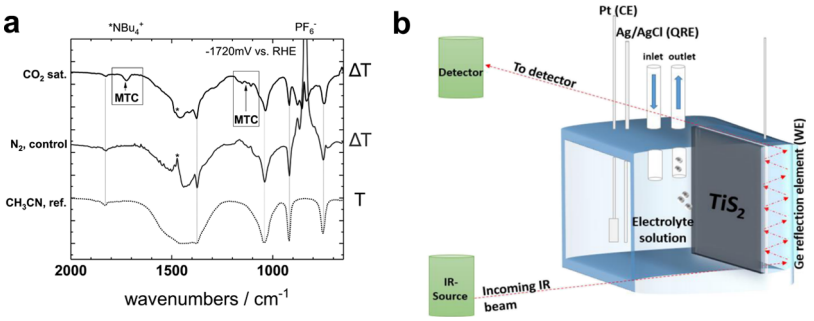

Figure 2. In situ FTIR on TiS_2 under electrochemical bias. (a) Survey of the differential absorption ($-\Delta T/T \propto$ Abs.) spectra of changes related either to monothiocarbonate (MCT) formation in the presence of CO_2 and changes related to solvent/electrolyte intercalation. The control spectra (N_2) show only features related to the electrolyte (NBu_4-PF_6) and solvent (reference spectrum of CH_3CN is included). (b) Schematic of the in situ FTIR setup. Internal reflection mode (ATR−FTIR) measurement using a germanium parallelepiped as a reflection element and the electrochemical flow cell mounted on top to elucidate the surface reaction on TiS_2 during CO_2 electroreduction.

these aspects merit further exploration to harness cathodic-activated (conductive) sulfur planes as powerful catalytic centers. In this context, TiS_2 represents a new frontier in electrochemical CO_2 conversion.

RESULTS AND DISCUSSION

We grew TiS_2 by atomic layer deposition (ALD) using sequential reaction of tetrakis(dimethylamido)titanium(IV) (TDMAT) and H_2S at 150 °C in vacuo.[33] The resulting thin films [200 nm (1T)-TiS_2] were deposited on glass, carbon paper, or germanium for the (spectro)electrochemical and electrical−structural studies. The Raman spectra (Figure 1a) revealed the fingerprint vibrational modes at 331 cm^{-1} (A_{1g})[34] related to the layered 2D (1T)-phase of TiS_2 (Figure 1c). We conducted resistivity ρ and Hall measurements: the thin films possessed similar values for resistances and Hall constants R_H compared to earlier reported bulk (1T)-TiS_2 crystals (3.7×10^{-3} Ω cm and 5.26×10^{-2} cm^3 C^{-1} at room temperature[4] and Hall mobility on the order of 13.6 cm^2 V^{-1} s^{-1}, respectively) (Figure 1b). The temperature coefficient of resistivity (TCR) was negative, and the carrier concentration was relatively constant as a function of temperature in the range of 10^{20} cm^{-3}. Both observations are signature characteristics of semimetals (Figure 1d and Supporting Information, Figure S1).

These results confirmed the high electrical conductivity of the TiS_2 thin films synthesized by ALD. As reported previously, the electrical properties of TiS_2 are found to be affected by exposure to ambient air.[37] Therefore, all reported experiments were conducted in oxygen-free atmosphere using organic electrolytes with oxygen levels below 1 ppm. The electrocatalytic experiments showed that TiS_2 works as an electrocatalytic layer on carbon paper as a conductive substrate (TiS_2-CP results are shown in Figure 3). The parasitic voltage drops as reported for MoS_2, and other TMDCs were negligible for the as-synthesized semimetal TiS_2.

DOI: 10.1021/acscatal.9b02872
ACS Catal. 2020, 10, 66−72

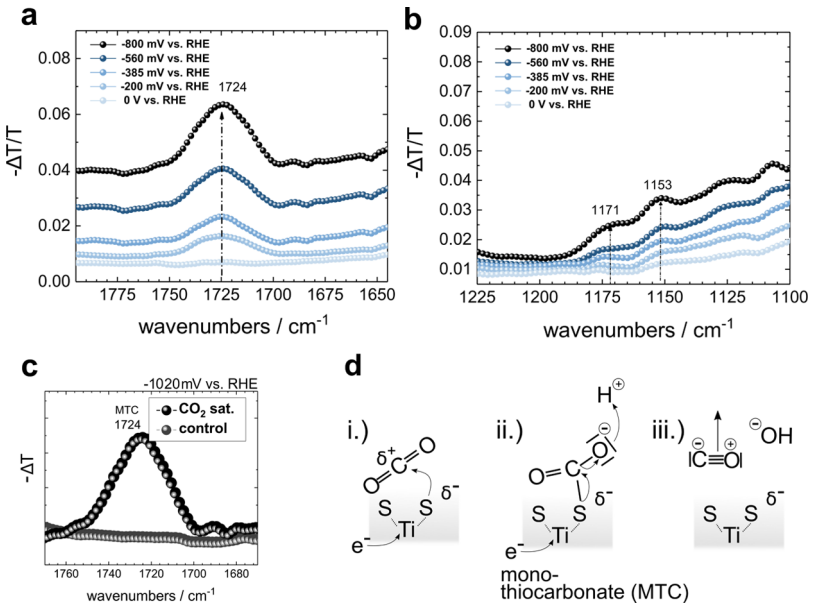

Figure 3. Detailed differential absorption and mechanism of CO_2RR on TiS_2. (a,b) Represent in situ differential absorption ($-\Delta T/T$) in the fingerprint regime showing the spectral changes related to monothiocarbonate (MTC, S−COO$^-$) carbonyl- and O−C−S stretch vibrations rising with cathodic bias. (c) Spectral comparison of MTC carbonyl at maximum reductive bias at −1020 mV vs RHE in CO_2-saturated electrolyte is compared to a control experiment without CO_2 (N_2-flushed). (d) Proposed mechanism of CO_2RR on TiS_2: (i) nucleophilic reaction of cathodic-biased sulfide to CO_2, (ii) formation of intermediate MTC, and (iii) further reduction including a proton to CO (and OH$^-$).

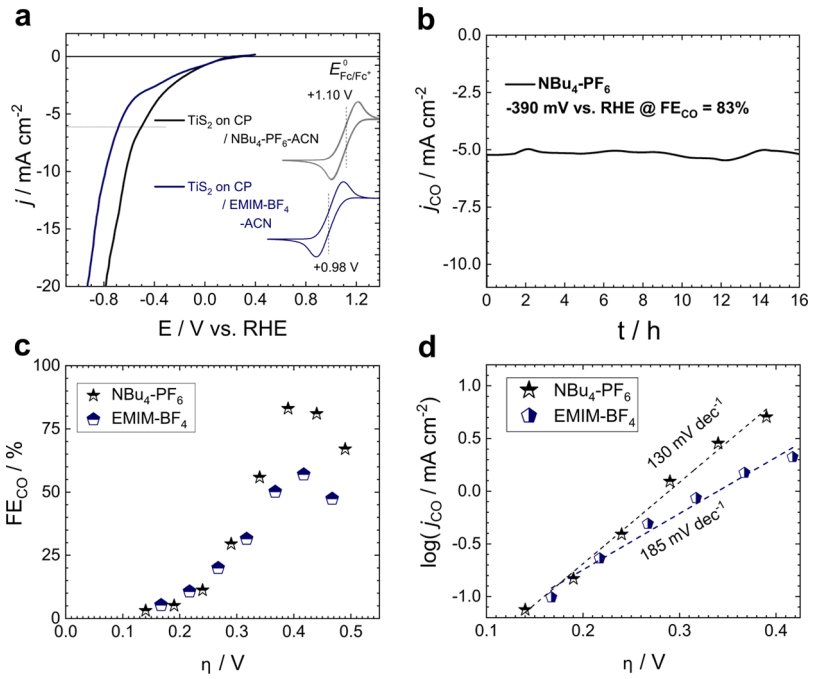

Figure 4. Electrocatalytic performance and stability analysis of CO_2-to-CO. (a) Cyclic voltammograms of TiS_2 in EMIM-BF_4 and NBu_4-PF_6. The inset shows the reference E_0 value for ferrocene/ferrocenium (Fc/Fc^+) standard. (b) CA (j_{CO}) scan for 16 h. (c) FE for CO shown in both electrolytes and (d) the corresponding CO Tafel slopes based on j_{CO}.

The main goal of this work was to harness the proven catalytic activity of TiS_2 for the CO_2RR. Earlier reports demonstrated that sulfides enhanced the catalyst performance.[9,16,26]

To reveal the reaction mechanism on TiS_2, we elucidated its surface reactivity by in situ FTIR spectroscopy (internal reflection mode, Figure 2b). We report the presence of carbonyl vibrations at 1724 cm^{-1} and O−C−S stretch oscillations at 1171 and 1153 cm^{-1} as soon as TiS_2 is under cathodic bias (Figure 3a,b). These features relate to monothiocarbonate features (MTC, S−COO$^-$) formed as CO_2−sulfide reaction intermediate.[38] The quantity of these features increased by rising the cathodic reduction potentials, in contrast to the relative intense, but constant solvent-related background features. MTC represents an intermediate capture state similar to metal complexes found on metallic surfaces necessary to accelerate further electroreduction.[8,38−41] A similar sulfide-based mechanism has been proposed for

DOI: 10.1021/acscatal.9b02872
ACS Catal. 2020, 10, 66−72

vacancies in the basal planes of 1T-phase TMD sulfides.[31,42−44] Particularly, Tsai et al.[31] proposed S−H intermediates at the cathode in analogy to our proposed MCT.

The control experiment without CO_2 (N_2 control experiment) showed no presence of MTC and only the spectral responses of electrolyte (NBu_4-PF_6) and solvent (CH_3CN) (Figures 3c and 2a). The mechanism proposed from the in situ spectral response is the nucleophilic attachment of sulfur to CO_2 enforced by the reducing environment (Figure 3d). A similar activation process has been reported in MoS_2 for hydrogen evolution reaction (HER) proposing intermediate H−S bonds. The corresponding intermediates in CO_2RR, formal MTC, as the competing HER intermediate S−H (5% hydrogen evolution) are indicated in the difference spectra: apart from (i) the carbonyl vibration (1724 cm^{-1}, Figure 3a) and (ii) the O−C−S stretch vibrations (1171 and 1153 cm^{-1}, Figure 3b), we found a spectral S−H peak at 2565 cm^{-1} (Supporting Information, Figure S8) that emerged from the competing HER.

The presence of a proton will lead the further decomposition of MTC to CO gas and hydroxyl (or water in neutral/acidic environment, Figure 3d). We denote that the as-formed CO can react further to formate, which we detect as an unavoidable byproduct (CO hydrolysis).[45,46]

We utilized in situ FTIR to test the stability window of TiS_2 and possible unwanted side reactions. In all our experiments, we used hybrid organic water electrolytes (water content is $1\%_{vol}$ in CH_3CN, 0.1 M NBu_4-PF_6) and reported reversibility up to −1020 mV versus reversible hydrogen electrode (RHE) (Figure 3c). The presence of water (or protons) is needed to allow the electroreduction of CO_2. In addition, water slightly increases the ionic conductivity, and it buffers the pH in acetonitrile at CO_2 saturation to 7.9. We did not find evidence of side reactions or decomposition of TiS_2 itself. In the control experiment without CO_2, the in situ FTIR spectra show only features relating to CH_3CN (included as a reference spectrum) and the electrolyte (NBu_4-PF_6) (Figure 3c, detailed spectra in the Supporting Information, Figures S5).

The electrochemical CO_2-to-CO conversion was measured in the same electrolyte system in an electrolysis cell using continuous chronoamperometry (CA) and cyclic voltammetry. The corresponding cell constants and the electrochemical surface area (ECSA) and the calibration of the reference electrode are presented in the Supporting Information (Figures S2 and S3) or as shown as an inset in Figure 4c. All Faradaic reduction currents are referenced to the ECSA and revealed the activity of TiS_2 as a potential CO_2 reduction electrocatalyst (i.e., j_{ECSA} = 20 mA cm^{-2} at −800 mV vs RHE) (Figure 4a). At −0.5 V versus RHE (corresponding to 0.39 V overpotential), we reached the maximum Faradaic efficiency (FE) of 83% at a Faradaic reduction current density of 5 mA cm^{-2} in 0.1 M NBu_4-PF_6 for CO (j_{CO}, Figure 4c). As a side product, formate (13%) and hydrogen (4%) are produced. We repeated the same experiments using an alternative ionic liquid−CH_3CN electrolyte (EMIM-BF_4 at $4\%_{vol}$, including $1\%_{vol}$ water). The presence of ionic liquid increased the electrolyte conductivity (Supporting Information, Figure S2 and Table 1) but decreased the selectivity for CO by a factor of 2 (maximum is 55%, Figure 4c). The main side product was here hydrogen (and negligible amounts of formate). In both electrolytes, there exists a general optimum potential range for CO at around 0.4 V overpotential. We performed the product analysis using gas (CO, H_2) and ion chromatography (formate) ex situ after continuous electrolysis (example shown in the Supporting Information, Figure S6). To demonstrate the electrode stability, we included an initial 16 h continuous electrosynthesis of CO (Figure 4b) and, similar to the in situ FTIR studies, found reversibility/stability with only negligible changes in the product yield and current. In particular, the spectral changes after electrode bias are related to the solvent (acetonitrile) and electrolyte intercalation inside TiS_2 as suggested by the in situ FTIR spectra (Figure 2a). In summary, we showed that TiS_2 possesses selectivity for CO_2RR producing mainly CO. From the experimental data on TiS_2 on carbon paper in two different electrolyte solutions (0.1 M NBu_4-PF_6 and EMIM-BF_4 at $4\%_{vol}$), we calculated the CO Tafel slopes (Figure 4d): the lowest slope was achieved using NBu_4-PF_6 at 130 mV dec^{-1}. In EMIM-BF_4, the j_{CO} and the Tafel slope increased to 185 mV dec^{-1}. In this context, TiS_2 behaves similarly as compared to earlier reports on 4d and 5d TMDCs investigated for CO_2RR and/or HER.[20,47−52] We estimated that the cathodic energy efficiency ($EE_{cathodic}$) is 64% at 0.39 V overpotential (eq 1, Gibb's free reaction energy ΔG_r for CO_2 splitting to CO and O_2 at 257.23 kJ mol^{-1}), the number of transferred electrons n = $2e^-$, the Faraday constant F, and FE for CO at 83%.

$$EE_{cathodic} = \frac{1}{nF} \cdot \frac{\Delta G_r}{\Delta G_r + nF \cdot \eta_{cathodic}} \cdot FE \quad (1)$$

A common observation from the present results on TiS_2 and other related dichalcogenide electrocatalysts is their compatibility with nonaqueous solvents.[16,20]

Table 1. Electrical Parameters at 300 K of Thin-Film and Bulk TiS_2

TiS_2 system	ρ/Ω cm	$R_H/cm^3\ C^{-1}$	$\mu_H/cm^2\ V^{-1}\ s^{-1}$	thickness
single crystal[a]	3.26×10^{-3}	5.50×10^{-2}	16.87	crystal
ALD thin film	3.77×10^{-3}	5.35×10^{-2}	14.17	200 nm

[a]Taken from Friend et al.[4]

CONCLUSIONS

Chalcogenide semiconductors have been frequently proposed as alternative systems in electrocatalysis to replace classic noble and precious metals, in particular for strategic aims in converting substantial amounts of anthropogenic emitted CO_2. However, compared to metals, the ultimate surface activities of chalcogenide semiconductors can be limited by poor electrical transport properties. We therefore found it compelling to elucidate the potential catalytic performance of the semimetallic dichalcogenide TiS_2 in the CO_2 reduction reaction. TiS_2 possesses an intrinsic electrical conductivity of approximately 260 S cm^{-1} and also offers cathodic reaction activity in sulfur batteries (to intercalate sodium and lithium ions) and for the HER. We transferred these insights now for CO_2RR and found excellent carbon conversion (CO and formate) efficiencies, that is combined Faradaic yield beyond 95% and overpotential below 0.4 mV at j_{CO} = 5 mA cm^{-2}. Interestingly, we reveal a sulfur−CO_2 intermediary monothiocarbonate that drives the reduction and leads to the reported high selectivity for CO. In particular, the catalytic activity of sulfur is a central aspect, which merits further exploration for rational design of electrocatalytic materials

DOI: 10.1021/acscatal.9b02872
ACS Catal. 2020, 10, 66−72

without consuming energy critical elements for large-scale CO_2 reduction.

EXPERIMENTAL SECTION

ALD Growth of TiS_2. TDMAT (99.99% Ti; Strem Chemicals) and H_2S are used as precursors in alternating pulsed ALD at a constant growth rate of 0.1 nm per cycle measured by DekTak. Nitrogen is used as a carrier gas (99.9999% pure, Carbagas) with a flow rate of 10 mL min^{-1} (sccm). TDMAT and H_2S are alternatively exposed to the deposition chambers using a 20 s exposure time and at 150 °C in vacuo at 2000 repeating loops. We used glass, carbon paper, and germanium as substrates.

Electrical Measurements. The final TiS_2 layer has a film thickness of 200 nm as measured by Dektak (Bruker). The films are brownish-opaque and conduct electricity. For the Hall measurements, we employ a van-der-Pauw specimen configuration. We use a shadow mask to deposit thin films of TiS_2 onto a patterned substrate. The electrical conductivity and the Hall constant are measured in Helium atmosphere between 300 and 100 K using a Lakeshore Hall measurement Setup 8400. The Hall parameters were set to 1 mA dc-current and 0.91 T.

Electrochemical Measurements. For the evaluation of the TiS_2 electrocatalyst, electrochemical studies were conducted in a standard three-electrode arrangement in an H-cell configuration. TiS_2 was set as the working electrode (WE), Ni as a counter electrode (CE), and Ag/AgCl as quasi reference electrode (QRE), all dipped into 0.1 M NBu_4-PF_6 or 4% EMIM-BF_4 in acetonitrile water with 1%$_{vol}$ (0.555 mol L^{-1}). The electrolyte solutions are purged with CO_2 for 1 h before characterization. The complete electrochemical system releases CO at the cathode compartment and evolves oxygen at the anode space (schematic in the Supporting Information, Figure S5). The WE and QRE were placed in the same compartment of the H-cell, whereas the CE is in the second zone to avoid any back oxidation at the CE. The anode and cathode compartments were separated by a glass frit as the membrane between the cells. The Ag/AgCl QRE is calibrated against the ferrocene/ferrocenium couple (Fc/Fc^+) as an internal reference. The actual applied potentials are consistently plotted versus the RHE. For this, we measured the pH using indicators and pH meters in both electrolytes and determined at 7.9 (NBu_4-PF_6) and 5.9 (4% EMIM-BF_4).[53] We calculated the RHE potential based on the calibrated QRE and the pH value (eq 2). Density functional theory calculations of the same electrolyte yielded similar values for the RHE (or, the standard hydrogen electrode, respectively).[54]

$$E_{RHE} = E_{QRE\ vs.Fc/Fc^+} + 0.641\ V + pH \cdot 0.0591\ V \quad (2)$$

All electrochemical experiments were performed using a JAISSLE Potentiostat Galvanostat IMP 88 PC, and the amount of CO gas was analyzed with TRACE Ultra Gas Chromatograph equipped with a thermal conductivity detector (TCD) (e.g., chromatogram for CO detection shown in the Supporting Information, Figure S7). The electrochemical experiments were performed in the glovebox atmosphere. The compartments of the H-cell were purged with N_2 and CO_2 before starting each experiment. For the analysis of the CO gas, 2 mL samples were taken from the headspace with a gastight syringe and injected to the gas chromatograph. Helium was used as the carrier gas with a flow rate of 20 mL min^{-1}. The TCD was kept at 200 °C. Capillary ion chromatography (CAP-IC) (Dionex ICS 5000, conductivity detector, AG19, CAP, 0.4 × 50 mm precolumn, AS19, CAP, 0.4 × 250 mm main column) with potassium hydroxide (KOH) as eluent for isocratic chromatography was adjusted for the analysis of liquid samples before and after controlled potential electrolysis. Before injection, the samples were diluted 1:20 with 18 MΩ cm of water. The CAP-IC injection was followed by injecting 1 mL of the diluted sample with a syringe. The electrochemical cell parameters and the ECSA are measured using electrochemical impedance spectroscopy carried out using a CompactStat (IVIUM). The impedance spectra were recorded between 100 and 0.1 MHz with an ac amplitude of 50 mV. From this, we derive an equivalent circuit and the electrolyte resistance R_{el}, the membrane resistance R_m, and the capacitance of the WE C_{WE} (summarized in the Supporting Information, Table S1, Figure S2). From the electrochemical capacitance, we derived the ECSA. To verify this decisive parameter, we crosschecked the ECSA using cyclic voltammogram sweeps of the WE at different scan rates (5 to 200 mV s^{-1}) (Supporting Information, Figure S3). The current densities reported in this manuscript are all normalized according to the ECSA.

In Situ FTIR. A flow cell is tightened inside a Bruker IFS/66 FTIR spectrometer, where the incident IR-beam is aligned using confocal mirrors through the germanium attenuated total reflection element (parallelepiped, multiple reflections at 45°, schematic in Figure 2). During the measurement of the voltammograms and FTIR spectra, the cell is continuously flushed with an electrolyte solution (0.1 M NBu_4-PF_6). Reference spectra and control cyclic voltammograms are recorded in a N_2- and CO_2-purged electrolyte (Supporting Information, Figure S6). The resulting in situ spectra at different electrochemical potentials are plotted as differential transmission ($-\Delta T$) and differential absorption ($-\Delta T/T \propto$ absorbance). The spectra show the spectroscopic changes induced by the electrochemical reaction on the surface. Negative spectroscopic signals correspond to a fading process and positive signals relate to an emerging, new features. The monothiocarbonate features represent the latter class (emerging).

ASSOCIATED CONTENT

Supporting Information

The Supporting Information is available free of charge at https://pubs.acs.org/doi/10.1021/acscatal.9b02872.

> Electrical transport measurements, material characterization, electrochemical and chromatographic characterization during CO_2 electrolysis, and further information on the in situ spectroelectrochemical probing (PDF)

AUTHOR INFORMATION

Corresponding Author

*E-mail: philipp.stadler@jku.at.

ORCID

Abdalaziz Aljabour: 0000-0002-0041-4591
Halime Coskun: 0000-0001-7284-2651
Xueli Zheng: 0000-0002-6800-2649
Edward H. Sargent: 0000-0003-0396-6495
Philipp Stadler: 0000-0001-6459-5574

DOI: 10.1021/acscatal.9b02872
ACS Catal. 2020, 10, 66−72

Present Addresses
[#]Department of Materials Science and Engineering, Stanford University, Stanford, CA 94305, USA.
[¶]Department of Chemical and Petroleum Engineering, University of Calgary, 2500 University Drive, NW Calgary, Alberta T2N 1N4, Canada.

Notes
The authors declare no competing financial interest.

■ ACKNOWLEDGMENTS

The authors thank the Government of Upper Austria within the Sabbatical program "Internationalization of the University of Linz" at the University of Toronto. The authors acknowledge the financial support of the Austrian Science Foundation (FWF I3822-N37, Sustainable Catalysis), the Linz Institute of Technology (LIT, LIT-2017-4-YOU-005, Biopolymer-based carbonate reduction) at the Johannes Kepler University Linz, and European Regional Development Fund (EFRE, IWB2014-2020, 2018-98299, Artificial Food).

■ REFERENCES

(1) Chu, S.; Cui, Y.; Liu, N. The path towards sustainable energy. *Nat. Mater.* **2017**, *16*, 16−22.
(2) Windle, C. D.; Perutz, R. N. Advances in molecular photocatalytic and electrocatalytic CO2 reduction. *Coord. Chem. Rev.* **2012**, *256*, 2562−2570.
(3) Chaturvedi, A.; Edison, E.; Arun, N.; Hu, P.; Kloc, C.; Aravindan, V.; Madhavi, S. Two Dimensional TiS 2 as a Promising Insertion Anode for Na-Ion Battery. *ChemistrySelect* **2018**, *3*, 524−528.
(4) Friend, R. H.; Jerome, D.; Liang, W. Y.; Mikkelsen, C.; Yoffe, A. D. Semimetallic character of TiSe 2 and semiconductor character of TiS 2 under pressure. *J. Phys. C: Solid State Phys.* **1977**, *10*, L705.
(5) Safaei, T. S.; Mepham, A.; Zheng, X.; Pang, Y.; Dinh, C.-T.; Liu, M.; Sinton, D.; Kelley, S. O.; Sargent, E. H. High-Density Nanosharp Microstructures Enable Efficient CO 2 Electroreduction. *Nano Lett.* **2016**, *16*, 7224−7228.
(6) Liu, M.; Pang, Y.; Zhang, B.; De Luna, P.; Voznyy, O.; Xu, J.; Zheng, X.; Dinh, C. T.; Fan, F.; Cao, C.; de Arquer, F. P. G.; Safaei, T. S.; Mepham, A.; Klinkova, A.; Kumacheva, E.; Filleter, T.; Sinton, D.; Kelley, S. O.; Sargent, E. H. Enhanced electrocatalytic CO2 reduction via field-induced reagent concentration. *Nature* **2016**, *537*, 382−386.
(7) Feaster, J. T.; Shi, C.; Cave, E. R.; Hatsukade, T.; Abram, D. N.; Kuhl, K. P.; Hahn, C.; Nørskov, J. K.; Jaramillo, T. F. Understanding Selectivity for the Electrochemical Reduction of Carbon Dioxide to Formic Acid and Carbon Monoxide on Metal Electrodes. *ACS Catal.* **2017**, *7*, 4822−4827.
(8) Gabardo, C. M.; Seifitokaldani, A.; Edwards, J. P.; Dinh, C.-T.; Burdyny, T.; Kibria, M. G.; O'Brien, C. P.; Sargent, E. H.; Sinton, D. Combined high alkalinity and pressurization enable efficient CO 2 electroreduction to CO. *Energy Environ. Sci.* **2018**, *11*, 2531−2539.
(9) Zhuang, T.-T.; Liang, Z.-Q.; Seifitokaldani, A.; Li, Y.; De Luna, P.; Burdyny, T.; Che, F.; Meng, F.; Min, Y.; Quintero-Bermudez, R.; Dinh, C. T.; Pang, Y.; Zhong, M.; Zhang, B.; Li, J.; Chen, P.-N.; Zheng, X.-L.; Liang, H.; Ge, W.-N.; Ye, B.-J.; Sinton, D.; Yu, S.-H.; Sargent, E. H. Steering post-C−C coupling selectivity enables high efficiency electroreduction of carbon dioxide to multi-carbon alcohols. *Nat. Catal.* **2018**, *1*, 421−428.
(10) De Luna, P.; Quintero-Bermudez, R.; Dinh, C.-T.; Ross, M. B.; Bushuyev, O. S.; Todorović, P.; Regier, T.; Kelley, S. O.; Yang, P.; Sargent, E. H. Catalyst electro-redeposition controls morphology and oxidation state for selective carbon dioxide reduction. *Nat. Catal.* **2018**, *1*, 103−110.
(11) Dinh, C.-T.; Burdyny, T.; Kibria, M. G.; Seifitokaldani, A.; Gabardo, C. M.; García de Arquer, F. P.; Kiani, A.; Edwards, J. P.; De Luna, P.; Bushuyev, O. S.; Zou, C.; Quintero-Bermudez, R.; Pang, Y.; Sinton, D.; Sargent, E. H. CO 2 electroreduction to ethylene via hydroxide-mediated copper catalysis at an abrupt interface. *Science* **2018**, *360*, 783−787.
(12) Shinagawa, T.; Larrazábal, G. O.; Martín, A. J.; Krumeich, F.; Pérez-Ramírez, J. Sulfur-Modified Copper Catalysts for the Electrochemical Reduction of Carbon Dioxide to Formate. *ACS Catal.* **2018**, *8*, 837−844.
(13) Zhou, Y.; Che, F.; Liu, M.; Zou, C.; Liang, Z.; De Luna, P.; Yuan, H.; Li, J.; Wang, Z.; Xie, H.; Li, H.; Chen, P.; Bladt, E.; Quintero-Bermudez, R.; Sham, T.-K.; Bals, S.; Hofkens, J.; Sinton, D.; Chen, G.; Sargent, E. H. Dopant-induced electron localization drives CO2 reduction to C2 hydrocarbons. *Nat. Chem.* **2018**, *10*, 974−980.
(14) Mariano, R. G.; McKelvey, K.; White, H. S.; Kanan, M. W. Selective increase in CO 2 electroreduction activity at grain-boundary surface terminations. *Science* **2017**, *358*, 1187−1192.
(15) Zhang, L.; Zhao, Z.-J.; Gong, J. Nanostructured Materials for Heterogeneous Electrocatalytic CO 2 Reduction and their Related Reaction Mechanisms. *Angew. Chem., Int. Ed.* **2017**, *56*, 11326−11353.
(16) Asadi, M.; Kumar, B.; Behranginia, A.; Rosen, B. A.; Baskin, A.; Repnin, N.; Pisasale, D.; Phillips, P.; Zhu, W.; Haasch, R.; Klie, R. F.; Král, P.; Abiade, J.; Salehi-Khojin, A. Robust carbon dioxide reduction on molybdenum disulphide edges. *Nat. Commun.* **2014**, *5*, 4470.
(17) Chhowalla, M.; Shin, H. S.; Eda, G.; Li, L.-J.; Loh, K. P.; Zhang, H. The chemistry of two-dimensional layered transition metal dichalcogenide nanosheets. *Nat. Chem.* **2013**, *5*, 263−275.
(18) Liu, Y.; Liang, C.; Wu, J.; Sharifi, T.; Xu, H.; Nakanishi, Y.; Yang, Y.; Woellne, C. F.; Aliyan, A.; Martí, A. A.; Xie, B.; Vajtai, R.; Yang, W.; Ajayan, P. M. Atomic Layered Titanium Sulfide Quantum Dots as Electrocatalysts for Enhanced Hydrogen Evolution Reaction. *Adv. Mater. Interfaces* **2018**, *5*, 1700895.
(19) Abbasi, P.; Asadi, M.; Liu, C.; Sharifi-Asl, S.; Sayahpour, B.; Behranginia, A.; Zapol, P.; Shahbazian-Yassar, R.; Curtiss, L. A.; Salehi-Khojin, A. Tailoring the Edge Structure of Molybdenum Disulfide toward Electrocatalytic Reduction of Carbon Dioxide. *ACS Nano* **2017**, *11*, 453−460.
(20) Asadi, M.; Kim, K.; Liu, C.; Addepalli, A. V.; Abbasi, P.; Yasaei, P.; Phillips, P.; Behranginia, A.; Cerrato, J. M.; Haasch, R.; Zapol, P.; Kumar, B.; Klie, R. F.; Abiade, J.; Curtiss, L. A.; Salehi-Khojin, A. Nanostructured transition metal dichalcogenide electrocatalysts for CO2 reduction in ionic liquid. *Science* **2016**, *353*, 467−470.
(21) Wang, Z.; Yang, G.; Zhang, Z.; Jin, M.; Yin, Y. Selectivity on Etching: Creation of High-Energy Facets on Copper Nanocrystals for CO 2 Electrochemical Reduction. *ACS Nano* **2016**, *10*, 4559−4564.
(22) Lu, Q.; Rosen, J.; Zhou, Y.; Hutchings, G. S.; Kimmel, Y. C.; Chen, J. G.; Jiao, F. A selective and efficient electrocatalyst for carbon dioxide reduction. *Nat. Commun.* **2014**, *5*, 3242.
(23) Oh, Y.; Vrubel, H.; Guidoux, S.; Hu, X. Electrochemical reduction of CO2 in organic solvents catalyzed by MoO2. *Chem. Commun.* **2014**, *50*, 3878.
(24) Oh, Y.; Hu, X. Ionic liquids enhance the electrochemical CO 2 reduction catalyzed by MoO 2. *Chem. Commun.* **2015**, *51*, 13698−13701.
(25) Piontek, S.; junge Puring, K.; Siegmund, D.; Smialkowski, M.; Sinev, I.; Tetzlaff, D.; Roldan Cuenya, B.; Apfel, U.-P. Bio-inspired design: bulk iron−nickel sulfide allows for efficient solvent-dependent CO 2 reduction. *Chem. Sci.* **2019**, *10*, 1075−1081.
(26) Zheng, X.; De Luna, P.; García de Arquer, F. P.; Zhang, B.; Becknell, N.; Ross, M. B.; Li, Y.; Banis, M. N.; Li, Y.; Liu, M.; Voznyy, O.; Dinh, C. T.; Zhuang, T.; Stadler, P.; Cui, Y.; Du, X.; Yang, P.; Sargent, E. H. Sulfur-Modulated Tin Sites Enable Highly Selective Electrochemical Reduction of CO 2 to Formate. *Joule* **2017**, *1*, 794−805.
(27) Gu, J.; Héroguel, F.; Luterbacher, J.; Hu, X. Densely Packed, Ultra Small SnO Nanoparticles for Enhanced Activity and Selectivity in Electrochemical CO 2 Reduction. *Angew. Chem., Int. Ed.* **2018**, *57*, 2943−2947.
(28) Gu, J.; Hsu, C.-S.; Bai, L.; Chen, H. M.; Hu, X. Atomically dispersed Fe3+ sites catalyze efficient CO2 electroreduction to CO. *Science* **2019**, *364*, 1091−1094.

DOI: 10.1021/acscatal.9b02872
ACS Catal. 2020, 10, 66−72

(29) Ivanovskaya, V. V.; Seifert, G. Tubular structures of titanium disulfide TiS2. *Solid State Commun.* **2004**, *130*, 175−180.
(30) Inoue, M.; Negishi, H. Interlayer spacing of 3d transition-metal intercalates of 1T-cadmium iodide-type titanium disulfide (TiS2). *J. Phys. Chem.* **1986**, *90*, 235−238.
(31) Tsai, C.; Li, H.; Park, S.; Park, J.; Han, H. S.; Nørskov, J. K.; Zheng, X.; Abild-Pedersen, F. Electrochemical generation of sulfur vacancies in the basal plane of MoS2 for hydrogen evolution. *Nat. Commun.* **2017**, *8*, 15113.
(32) Quan, F.; Zhong, D.; Song, H.; Jia, F.; Zhang, L. A highly efficient zinc catalyst for selective electroreduction of carbon dioxide in aqueous NaCl solution. *J. Mater. Chem. A* **2015**, *3*, 16409−16413.
(33) Pore, V.; Ritala, M.; Leskelä, M. Atomic Layer Deposition of Titanium Disulfide Thin Films. *Chem. Vap. Deposition* **2007**, *13*, 163−168.
(34) Yuwen, L.; Yu, H.; Yang, X.; Zhou, J.; Zhang, Q.; Zhang, Y.; Luo, Z.; Su, S.; Wang, L. Rapid preparation of single-layer transition metal dichalcogenide nanosheets via ultrasonication enhanced lithium intercalation. *Chem. Commun.* **2015**, *52*, 529−532.
(35) Conroy, L. E.; Park, K. C. Electrical properties of the Group IV disulfides, titanium disulfide, zirconium disulfide, hafnium disulfide and tin disulfide. *Inorg. Chem.* **1968**, *7*, 459−463.
(36) Kam, K.-K. Electrical properties of WSe_2, WS_2, $MoSe_2$, MoS_2, and their use as photoanodes in a semiconductor liquid junction solar cell, Ph.D. Thesis, Iowa State University, 1982.
(37) Whittingham, M. S.; Panella, J. A. Formation of stoichiometric titanium disulfide. *Mater. Res. Bull.* **1981**, *16*, 37−45.
(38) Erben, M. F.; Boese, R.; Della Védova, C. O.; Oberhammer, H.; Willner, H. Toward an Intimate Understanding of the Structural Properties and Conformational Preference of Oxoesters and Thioesters: Gas and Crystal Structure and Conformational Analysis of Dimethyl Monothiocarbonate, CH 3 OC(O)SCH 3. *J. Org. Chem.* **2006**, *71*, 616−622.
(39) Al-Hosney, H. A.; Carlos-Cuellar, S.; Baltrusaitis, J.; Grassian, V. H. Heterogeneous uptake and reactivity of formic acid on calcium carbonate particles: a Knudsen cell reactor, FTIR and SEM study. *Phys. Chem. Chem. Phys.* **2005**, *7*, 3587.
(40) Andrei, H.-S.; Nizkorodov, S. A.; Dopfer, O. IR Spectra of Protonated Carbonic Acid and Its Isomeric H3O+CO2 Complex. *Angew. Chem., Int. Ed.* **2007**, *46*, 4754−4756.
(41) Phillips, K. R.; Katayama, Y.; Hwang, J.; Shao-Horn, Y. Sulfide-Derived Copper for Electrochemical Conversion of CO 2 to Formic Acid. *J. Phys. Chem. Lett.* **2018**, *9*, 4407−4412.
(42) Huang, Y.; Nielsen, R. J.; Goddard, W. A. Reaction Mechanism for the Hydrogen Evolution Reaction on the Basal Plane Sulfur Vacancy Site of MoS 2 Using Grand Canonical Potential Kinetics. *J. Am. Chem. Soc.* **2018**, *140*, 16773−16782.
(43) Voiry, D.; Fullon, R.; Yang, J.; de Carvalho Castro e Silva, C.; Kappera, R.; Bozkurt, I.; Kaplan, D.; Lagos, M. J.; Batson, P. E.; Gupta, G.; Mohite, A. D.; Dong, L.; Er, D.; Shenoy, V. B.; Asefa, T.; Chhowalla, M. The role of electronic coupling between substrate and 2D MoS 2 nanosheets in electrocatalytic production of hydrogen. *Nat. Mater.* **2016**, *15*, 1003−1009.
(44) Ji, Y.; Nørskov, J. K.; Chan, K. Scaling Relations on Basal Plane Vacancies of Transition Metal Dichalcogenides for CO 2 Reduction. *J. Phys. Chem. C* **2019**, *123*, 4256−4261.
(45) Yasaka, Y.; Yoshida, K.; Wakai, C.; Matubayasi, N.; Nakahara, M. Kinetic and Equilibrium Study on Formic Acid Decomposition in Relation to the Water-Gas-Shift Reaction. *J. Phys. Chem. A* **2006**, *110*, 11082−11090.
(46) Hietala, J.; Vuori, A.; Johnsson, P.; Pollari, I.; Reutemann, W.; Kieczka, H. *Ullmann's Encyclopedia of Industrial Chemistry*; Wiley-VCH Verlag GmbH & Co. KGaA: Weinheim, Germany, 2016; pp 1−22.
(47) Xu, C.; Peng, S.; Tan, C.; Ang, H.; Tan, H.; Zhang, H.; Yan, Q. Ultrathin S-doped MoSe 2 nanosheets for efficient hydrogen evolution. *J. Mater. Chem. A* **2014**, *2*, 5597−5601.
(48) Tan, C.; et al. Preparation of High-Percentage 1T-Phase Transition Metal Dichalcogenide Nanodots for Electrochemical Hydrogen Evolution. *Adv. Mater.* **2018**, *30*, 1705509.
(49) Zhang, X.; Lai, Z.; Zhang, H. Doping-induced phase transition enables better electrocatalysts. *Sci. China Mater.* **2018**, *61*, 1623−1624.
(50) Lu, Q.; Yu, Y.; Ma, Q.; Chen, B.; Zhang, H. 2D Transition-Metal-Dichalcogenide-Nanosheet-Based Composites for Photocatalytic and Electrocatalytic Hydrogen Evolution Reactions. *Adv. Mater.* **2016**, *28*, 1917−1933.
(51) Li, Z.; Zhang, X.; Cheng, H.; Liu, J.; Shao, M.; Wei, M.; Evans, D. G.; Zhang, H.; Duan, X. Confined Synthesis of 2D Nanostructured Materials toward Electrocatalysis. *Adv. Energy Mater.* **2019**, 1900486.
(52) Shi, J.; Wang, X.; Zhang, S.; Xiao, L.; Huan, Y.; Gong, Y.; Zhang, Z.; Li, Y.; Zhou, X.; Hong, M.; Fang, Q.; Zhang, Q.; Liu, X.; Gu, L.; Liu, Z.; Zhang, Y. Two-dimensional metallic tantalum disulfide as a hydrogen evolution catalyst. *Nat. Commun.* **2017**, *8*, 958.
(53) Coskun, H.; Aljabour, A.; De Luna, P.; Farka, D.; Greunz, T.; Stifter, D.; Kus, M.; Zheng, X.; Liu, M.; Hassel, A. W.; Schöfberger, W.; Sargent, E. H.; Sariciftci, N. S.; Stadler, P. Biofunctionalized conductive polymers enable efficient CO 2 electroreduction. *Sci. Adv.* **2017**, *3*, No. e1700686.
(54) Costentin, C.; Drouet, S.; Robert, M.; Savéant, J.-M. A Local Proton Source Enhances CO2 Electroreduction to CO by a Molecular Fe Catalyst. *Science* **2012**, *338*, 90−94.

DOI: 10.1021/acscatal.9b02872
ACS Catal. 2020, 10, 66−72